Quasiperiodic potential induced corner states in a quadrupolar insulator

Srijata Lahiri* and Saurabh Basu
Department of Physics, Indian Institute of Technology Guwahati-Guwahati, Assam 781039, India

(Received 25 June 2024; revised 30 July 2024; accepted 1 August 2024; published 19 August 2024)

We systematically investigate the topological and localization properties of a quadrupolar insulator represented by the celebrated Benalcazar-Bernevig-Hughes model in the presence of quasiperiodic (QP) disorder instilled in its hopping amplitude. While disorder can be detrimental to the existence of the topological order in a system, we observe the emergence of a disorder-driven topological phase where the original (clean) system demonstrates trivial behavior. This phenomenon is confirmed by the re-emergence of zero-energy states in the band structure together with a nonzero bulk quadrupole moment, which in turn establishes the bulk-boundary correspondence (BBC). Furthermore, the distribution of the excess electronic charge shows a pattern that is reminiscent of the bulk quadrupole topology. To delve into the localization properties of the midband states, we compute the inverse participation and normalized participation ratios. It is observed that the in-gap states become critical (multifractal) at the point that discerns a transition from a topological localized to a trivial localized phase. Finally, we carry out a similar investigation to ascertain the effect of the QP disorder on the quadrupolar insulator when the model exhibits topological properties in the absence of disorder. Again, we note a multifractal behavior of the eigenstates in the vicinity of the transition.

DOI: 10.1103/PhysRevB.110.075422

I. INTRODUCTION

Topological insulators (TIs) have represented an area of supreme interest in the field of condensed matter physics for over a decade, being the cradle of exotic phenomena like anomalous quantum Hall and quantum spin Hall phases [1–4]. TIs correspond to systems in d dimensions that exhibit insulating properties in the bulk while hosting robust metallic surface states at the $(d-1)$-dimensional boundary. The field of topology has been extensively explored from both theoretical and experimental fronts, providing numerous material candidates that vividly exhibit robust boundary features. Examples include the seminal work by Bernevig *et al.* [5] and König *et al.* [6] on the quantum spin Hall effect in CdTe/HgTe quantum wells, followed by several works on Dirac and Weyl semimetals [7–10], topological superconductors [11,12], and topological crystalline insulators [13,14].

Currently, higher-order TIs (HOTIs) have garnered considerable interest, as a noteworthy extension to the field of conventional first-order TIs [15–20]. HOTIs feature robust topological states at boundaries of dimensions less than $d-1$ for a topologically nontrivial d-dimensional bulk, leading to the formation of corner states in two-dimensional (2D) and corner/hinge states in three-dimensional (3D) systems. While experimental evidence of real material candidates featuring higher-order states in 2D remains absent, evidence of second-order topology has been found in 3D in bismuth [21] and stacked bismuth halide chains [22].

TIs with quantized quadrupole moments require a special mention in the field of higher-order topology. The quadrupolar TIs (QTIs) have attracted significant interest as prime examples of HOTIs, where the bulk invariant (quadrupole moment) leads to the accumulation of quantized charge at the zero-dimensional (0D) corners of a 2D supercell [23–25]. These 0D corner modes act as signatures of the unconventional bulk-boundary correspondence specific to the higher-order phase. While classical electromagnetic theory dictates an equality in the magnitude of the edge dipole moment, corner charge, and bulk quadrupole moment in the absence of free dipoles in the system, it was shown in Ref. [26] that quadrupole topology that violates the *classical relation* can also exist [27]. Such systems are referred to as type-II QTIs. Additionally, authors of a recent work have described a quadrupolar insulator that does not show zero-energy states in its energy spectrum but does exhibits midgap states in the spectra corresponding to the entanglement [28]. It is to be noted that the quadrupole moment is a direct extension to the higher order of the Berry phase machinery that classifies band topology. QTIs have been explored extensively under several backdrops, namely, periodic drive, non-hermiticity, and random disorder. Floquet QTIs, which exhibit the presence of corner modes characterized by a quantized Floquet quadrupole moment, have been recently studied [29,30]. Furthermore, trivial lattices, when subjected to intricate external losses can give rise to quadrupole topology characterized by biorthogonal nested Wilson loop spectra [31]. Additionally, in a pioneering work by Li *et al.* [32], it was shown that quadrupole topology can be successfully defined in the presence of disorder provided the system satisfies chiral symmetry. This opened up a plethora of research on the interplay of disorder and topology in tight-binding systems including the work done by Yang *et al.* [33,34], where random on-site disorder revived the higher-order topological phase in a quadrupolar insulator beyond its

*Contact author: srijata.lahiri@iitg.ac.in

topological regime. Motivated by this interplay caused by the conjunction between random disorder and topology, we study the Benalcazar-Bernevig-Hughes (BBH) model, which is a prototypical example of a quadrupolar insulator hosting 0D corner modes, under the action of quasiperiodic (QP) disorder introduced into the hopping potential. Incommensurate or QP potential constitutes a bridge between the completely periodic and completely random regime, thus manifesting a manifold of phases not exhibited by either limit [35,36]. While clean systems possessing translational invariance host periodic Bloch states, the presence of completely random disorder leads to absolute localization of states for arbitrarily small disorder strength in one dimension (1D) and 2D. However in 3D, the existence of a mobility edge is possible that represents a critical point of separation in energy between the localized and the extended states [37]. QP systems, on the other hand, can achieve such a transition even in 1D. This was beautifully exhibited in the Aubry-André (AA) model, which represents one of the most popular examples of a QP lattice [38,39]. It introduces an incommensurate on-site potential in a tight-binding 1D chain with nearest-neighbor hopping amplitudes. The 1D AA model exhibits a complete localization-delocalization transition at a specific value of the disorder strength which was unforeseen in 1D system with random disorder. It should be mentioned here that, while higher-order topology in a 2D Aubry-André-Harper model has been studied [40], the complete effect of the QP disorder on the topology of the system, including its capacity to restore a topological phase in the otherwise trivial regime, has not been explored in detail. Our primary motivation in this paper was therefore to address the effect of QP on the BBH model, which is a well-known quadrupolar insulator, and study the different topological phases that emerge due to this interplay.

The paper is structured as follows. In Sec. II, we introduce the Hamiltonian of the original BBH model followed by a discussion on its topology and boundary modes. In Sec. III, we study the effect of the QP disorder on the topology of the model, starting from a regime where the system is trivial in the clean limit. In Sec. IV, a similar analysis is done on the system, this time residing within the regime that is topological in the clean limit. We also explore several indicators of the localization phenomena to decipher the confinement of the topological states. Finally, we conclude in Sec. IV.

II. BBH MODEL

The existence of a QTI requires at least two occupied bands in addition to the presence of crystalline symmetries that quantize the quadrupole moment [24]. The BBH model, which is a four-band insulator, abiding by the aforementioned criteria, is one of the most well-studied examples of a QTI. The Hamiltonian for the BBH model is given as

$$\begin{aligned} H(k_x, k_y) = {} & [\gamma + \lambda\cos(k_x)]\tau_1\sigma_0 - \lambda\sin(k_x)\tau_2\sigma_3 \\ & - [\gamma + \lambda\cos(k_y)]\tau_2\sigma_2 \\ & - \lambda\sin(k_y)\tau_2\sigma_1 + \delta\tau_3\sigma_0. \end{aligned} \tag{1}$$

The unit cell comprises four sublattices, as shown in Fig. 1. A magnetic field penetrates the system, uniformly bestowing a total of π flux per plaquette. Here, γ and λ correspond

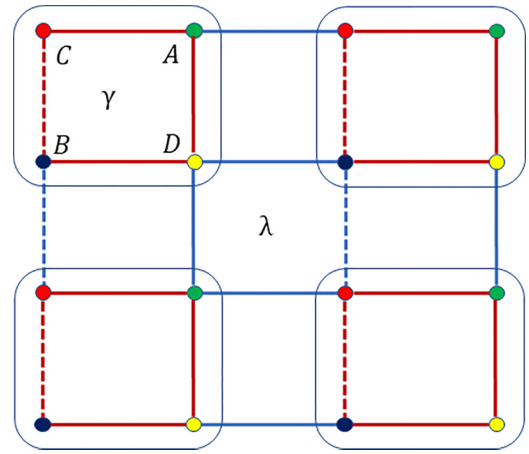

FIG. 1. A schematic diagram of the Benalcazar-Bernevig-Hughes (BBH) model is shown. Each unit cell consists of four sublattices marked as A, B, C, and D. The intracellular hopping amplitude is shown by γ, whereas λ represents the intercellular hopping. The dotted lines correspond to a negative hopping amplitude pertaining to a flux of magnitude π that penetrates each plaquette.

to the intracell and intercell hoppping, respectively, and δ corresponds to the on-site potential and is kept infinitesimally ~ 0. Furthermore, the Pauli matrices τ and σ correspond to the orbital degrees of freedom. The band structure of the BBH model shows the existence of zero-energy modes (Fig. 2) characterized by a topological quadrupole moment for $|\frac{\gamma}{\lambda}| < 1$ [Fig. 3(a)]. The quadrupole moment is protected by the dual mirror symmetry M_x and M_y such that

$$M_\alpha H(k_x, k_y) M_\alpha^\dagger = H(M_\alpha \mathbf{k}), \quad \alpha \in x, y, \tag{2}$$

where $M_x\mathbf{k} = (-k_x, k_y)$ and $M_y\mathbf{k} = (k_x, -k_y)$. At $\delta = 0$ and $|\frac{\gamma}{\lambda}| < 1$, four degenerate zero-energy in-gap corner states

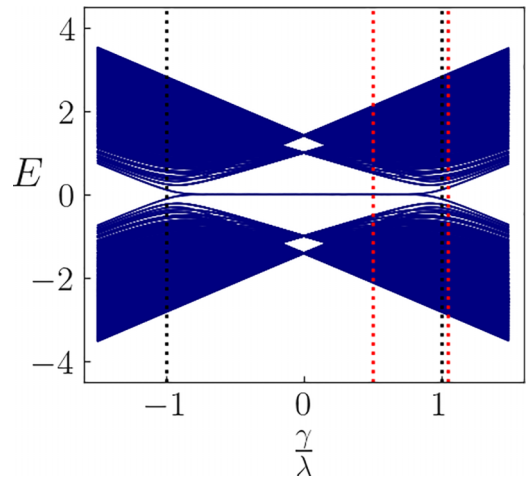

FIG. 2. The band structure of the original Benalcazar-Bernevig-Hughes (BBH) model is plotted as a function of $\frac{\gamma}{\lambda}$. Robust midband states, affixed at zero energy, are observed for $|\frac{\gamma}{\lambda}| < 1$. The size of the lattice has been considered 40×40. The black lines denote the quadrupolar topological regime, whereas the red lines mark the points $\frac{\gamma}{\lambda} = 1.05$ and 0.5, for which the effect of disorder on the topology of the system is studied.

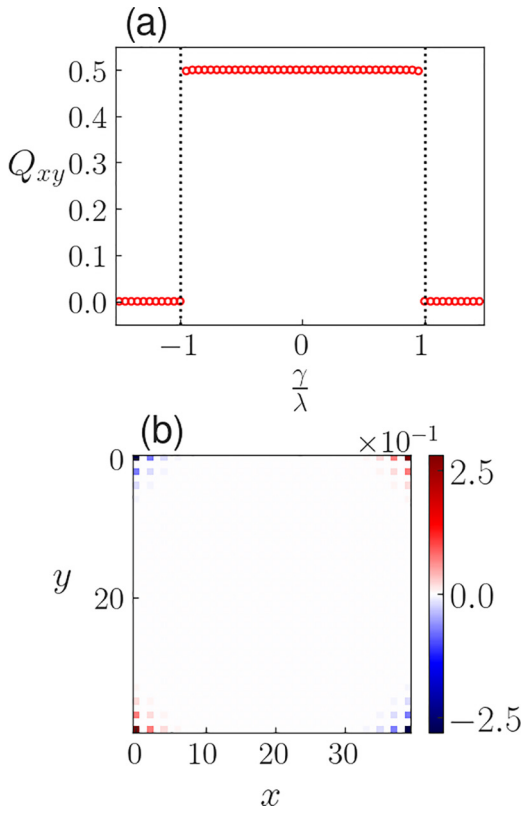

FIG. 3. (a) The quadrupole moment Q_{xy} plotted as a function of $\frac{\gamma}{\lambda}$ shows a nontrivial value of 0.5, for $|\frac{\gamma}{\lambda}| < 1$. This confirms the bulk-boundary correspondence in the second-order quadrupole topological insulator phase. (b) The excess charge distribution in the system for $|\frac{\gamma}{\lambda}| < 1$, shows a unique pattern with an excess and deficit of charge accumulation at the alternate corners. More specifically, here, $\gamma = 0.5$, and λ has been taken to be 1 throughout.

emerge. On increasing the value of δ slightly, the degeneracy of the zero-energy states is lifted, and the system exhibits a unique charge density pattern at the corners of a square supercell which is reminiscent of the bulk quadrupole moment [Fig. 3(b)].

We now elaborate on the evaluation of the charge distribution, as it corresponds to the most vital signature of second-order topology in the BBH model. The site-resolved charge distribution is evaluated from the eigenvectors of the real-space Hamiltonian written in the basis of the lattice sites. On exact diagonalization of the real-space Hamiltonian, the charge distribution over the lattice can be evaluated by summing over the probability distributions of the eigenvectors within the occupied subspace. Furthermore, any orbital or spin degree of freedom pertaining to individual lattice sites for each eigenvector must be summed over. The charge excess at different lattice sites is now obtained by calculating the difference between the charge distribution at individual sites and the average charge distribution. This accumulated charge at the corners of the BBH supercell is quantized to a value of $\pm\frac{e}{2}$. In the regime $|\frac{\gamma}{\lambda}| > 1$, however, the zero-energy corner states vanish, and the second-order topology in the system is lost. It should be mentioned here that, for the emergence of a quantized quadrupole moment (and hence a quantized amount of excess charge at the corners), it is necessary for the reflection operators, that is, M_x and M_y, to anticommute. To calculate the quadrupole moment Q_{xy}, we now resort to the formalism prescribed in Ref. [41], which provides an alternative approach to the nested Wilson loop method. In this method, the real-space charge distribution is employed to evaluate Q_{xy} as follows [32]:

$$Q_{xy} = \frac{1}{2\pi}\mathrm{Im}\ \ln[\det(U^\dagger \hat{q} U)\sqrt{\det(\hat{q}^\dagger)}]. \tag{3}$$

Here, $\hat{q} = \exp[2\pi i \hat{Q}_{xy}]$, where $\hat{Q}_{xy} = \frac{\hat{x}\hat{y}}{L_x L_y}$, and $\hat{x}(\hat{y})$ and $L_x(L_y)$ correspond to the position operator and the length of the system, respectively, in the $x(y)$ direction. Additionally, the matrix U is constructed by columnwise packing all the occupied eigenstates of the BBH Hamiltonian under periodic boundary conditions (PBCs). It is observed that the quadrupole moment exhibits a quantized value of $\frac{1}{2}$, for the regime $|\frac{\gamma}{\lambda}| < 1$, while becoming trivial for $|\frac{\gamma}{\lambda}| > 1$. It should be mentioned here that a direct manifestation of $Q = \frac{1}{2}$ at the boundary is the accumulation of excess corner charges of magnitude $\pm\frac{e}{2}$. This establishes the refined bulk-boundary correspondence (BBC) in the second-order topological phase.

III. DISORDERED BBH MODEL

A. Clean limit: Trivial phase

1. Topological properties of the model

Disorder possesses the capacity to generate topological phases when introduced in suitable systems. To explore this interplay, we introduce QP disorder in the intracellular hopping amplitude of the BBH model such that

$$\gamma_{x_n} = \gamma + W\cos(2\pi\beta x_n + \phi),$$
$$\gamma_{y_n} = \gamma + W\cos(2\pi\beta y_n + \phi). \tag{4}$$

Here, $\gamma_{x_n}(x_n)$ and $\gamma_{y_n}(y_n)$ correspond to the hopping amplitude (position coordinate) along the x and y directions, respectively, for the nth lattice site. The intercellular hopping amplitude λ is, however, kept fixed at 1, and W corresponds to the strength of the disorder. We have kept β equal to $\frac{1}{\sqrt{2}}$, which is responsible for the introduction of incommensurability into the system, and ϕ corresponds to the phase of the disorder which is kept 0 throughout. It may be noted that different variants of the QP potential exist in the literature; however, the one considered here is the most common. We plot the quadrupole moment Q_{xy} as a function of the disorder amplitude W and the intracellular hopping amplitude γ (Fig. 4). The invariant has been calculated on a 40×40 lattice, and a comparison between different system sizes is done later. It should be mentioned here that the QP disorder has been introduced into the model such that the original chiral symmetry of the system, which is given by $\tau_3 \otimes \sigma_0$, is kept intact. This is crucial for the quantization of the quadrupole moment, as mentioned in Ref. [32]. Furthermore, the nested Wilson loop approach fails here, owing to the lack of translational symmetry in the crystal due to the inclusion of disorder potential. We observe in Fig. 4 that the system undergoes a transition into the second-order topological phase characterized by the quadrupole moment in the regime $\frac{\gamma}{\lambda} > 1$ (which is completely trivial in the clean

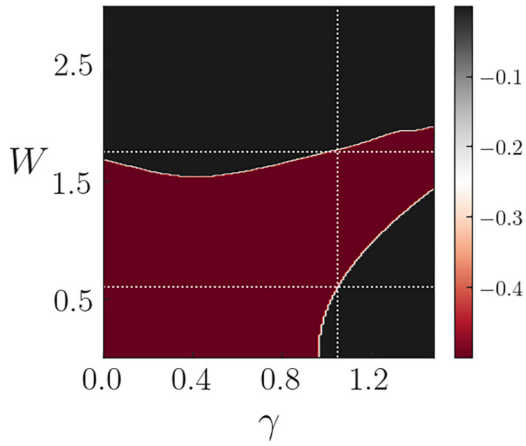

FIG. 4. The variation of the quadrupole moment Q_{xy} as a function of the disorder strength W and the intracellular hopping parameter γ is plotted. The vertical dotted line corresponds to $\gamma = 1.05$, which represents the trivial limit in the clean case. The horizontal lines mark the regime where the system enters a disorder-driven second-order topological phase.

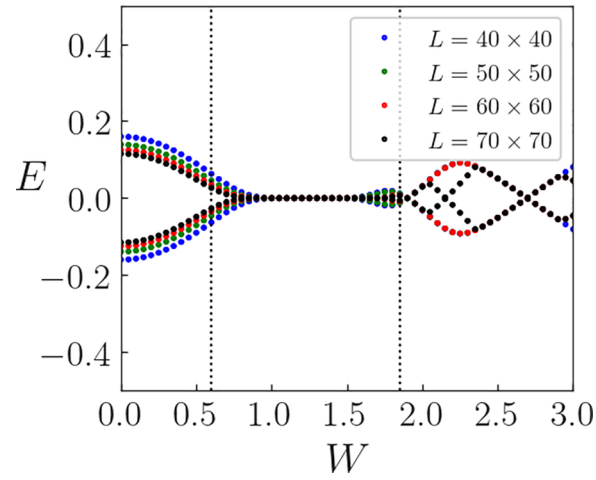

FIG. 6. The energy eigenvalues of the midband states are plotted as a function of W. The dotted lines correspond to $W = 0.6$ and 1.75, which demarcate the disorder-driven topological phase from the trivial one. We observe that the midband states are affixed at zero energy in the topological regime. Here, $\frac{\gamma}{\lambda} = 1.05$.

case), for a finite nonzero value of the disorder strength. This implies that the QP disorder restores the second-order topology in the BBH model for a finite range of the disorder strength prior to completely trivializing the system. We now fix the value of the ratio $\frac{\gamma}{\lambda}$ at 1.05, which corresponds to the trivial limit ($Q_{xy} = 0$) in the clean case. Figure 5 shows the plot of the quadrupole moment solely as a function of the disorder strength. The plot shows a nontrivial value of Q for W ranging roughly from 0.6 to 1.75. The band structure of the disordered BBH model under open boundary conditions (OBCs) also shows the formation of zero-energy states in this region (Fig. 6). The agreement between the quadrupole moment and emergence of zero-energy states thus confirms the restoration of the refined BBC in the disorder-induced second-order topological phase. Furthermore, the

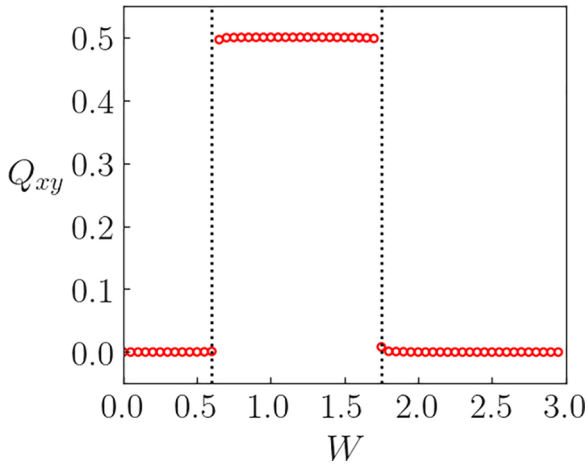

FIG. 5. The quadrupole moment Q_{xy} indicates a nontrivial topology in the regime $W \in (0.6, 1.75)$, thus proving the restoration of bulk-boundary correspondence (BBC) by the quasiperiodic disorder. Here, we have taken $\frac{\gamma}{\lambda} = 1.05$, which corresponds to the trivial limit in the clean case.

excess charge density is plotted for different values of the disorder strength corresponding to the trivial and topological phases (Fig. 7). It is observed that the accumulation of charge densities at the corners of a square supercell is negligible when $W > 1.75$ and $W < 0.6$, indicative of a trivial topology. However, for $0.6 < W < 1.75$, the distribution of excess charge at the corners shows a pattern which is suggestive of the inherent bulk quadrupole topology.

2. Localization study

In this section, we embark upon the localization properties of the disordered BBH model. For this purpose, two diagnostic quantities, namely, the inverse participation ratio (IPR) and the normalized participation ratio (NPR), are investigated. The IPR can be mathematically represented as [42]

$$\mathrm{IPR}^m = \sum_{i=1,\alpha}^{N} \left|u^m_{i,\alpha}\right|^4, \quad \alpha \in A, B, C, D, \tag{5}$$

where m denotes the band index, and N denotes the total number of lattice sites in the square supercell. Here, $|u^m\rangle$ corresponds to the mth eigenstate of the disordered BBH Hamiltonian under OBCs. IPR represents an important signature of localization in condensed matter systems which tends to 0 for extended states while being finite for localized states (approaches 1 in the thermodynamic limit). The NPR, on the other hand, can be represented as [43]

$$\mathrm{NPR} = \frac{1}{N} \frac{1}{\sum_{i=1,\alpha}^{N} \left|u^m_{i,\alpha}\right|^4}, \quad \alpha \in A, B, C, D, \tag{6}$$

where the symbols represent the same quantities as mentioned earlier. The NPR assumes a finite nonzero value in the extended case while tending to 0 in the thermodynamic limit for the localized case. More precisely, the behavior of IPR in

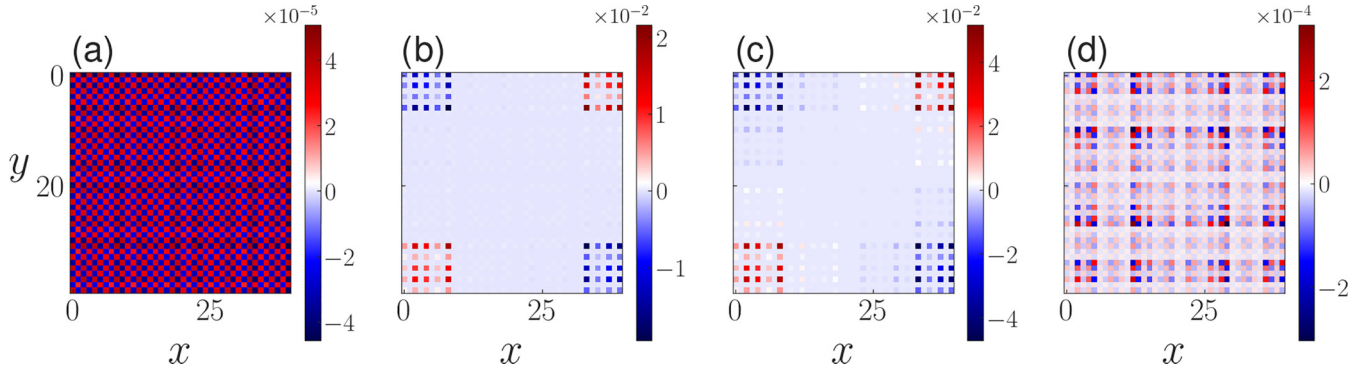

FIG. 7. The excess charge distribution has been plotted for (a) $W = 0.3$, (b) $W = 1.0$, (c) $W = 1.2$, and (d) $W = 2.1$, respectively. The distribution shows no quadrupolar pattern in the trivial regime, that is, $W < 0.6$ and $W > 1.75$, as shown in (a) and (d). However, a distribution pattern like Fig. 3(b) is seen in the topological regime [(b) and (c)].

localized and extended systems can be given as [44]

$$\text{IPR} \sim \begin{cases} \frac{1}{L^D}, & \text{extended systems,} \\ O(1), & \text{localized systems,} \end{cases} \tag{7}$$

However, NPR shows a contrasting feature in the two regimes:

$$\text{NPR} \sim \begin{cases} O(1), & \text{extended systems,} \\ \frac{1}{L^D}, & \text{localized systems,} \end{cases} \tag{8}$$

We plot the average value of IPR and NPR (denoted by $\langle \text{IPR} \rangle$ and $\langle \text{NPR} \rangle$) for the four degenerate zero-energy states (Fig. 8). It is observed that the values of $\langle \text{IPR} \rangle$ remain ~ 0 until roughly $W = 0.6$, beyond which it assumes a finite nonzero value. Around $W = 1.75$, the value of $\langle \text{IPR} \rangle$ decreases, before finally increasing again. This indicates that the four midband states are delocalized when $W < 0.6$, which is like what happens in the clean case for $|\frac{\gamma}{\lambda}| > 1$. Beyond $W = 0.6$, the disorder-driven quadrupole phase affixes these midband states at zero energy and localizes them. For higher values of the disorder strength (beyond $W = 1.75$), the states are no longer at zero energy and are not topological. The decrease in the value of IPR around $W = 1.75$ indicates a delocalization caused by the phase transition that destroys the quadrupole topology in the system. Much beyond $W = 1.75$, localization sets in due to the larger values of the disorder strength. The system is then in a trivial Anderson localized phase. The variation of $\langle \text{NPR} \rangle$ as a function of W [Fig. 8(b)] provides similar information.

Another widely investigated concept in the study of localization is the fractal dimension. Despite IPR and NPR being excellent signatures of localization/delocalization in a system, they are not individually efficient indicators of multifractality. Therefore, to investigate the existence of possible multifractality in the system, we calculate the fractal dimension D_2 which assumes a value close to D in the thermodynamic limit for the extended states, while being 0 for the localized states. However, in the multifractal phase, $D_2 \in (0, D)$. Here, D refers to the physical dimensionality of the system, which is 2 in our case. The mathematical representation of D_2 can be given as [43]

$$D_2 = -\lim_{L\to\infty} \frac{\ln(\text{IPR})}{\ln(L)}. \tag{9}$$

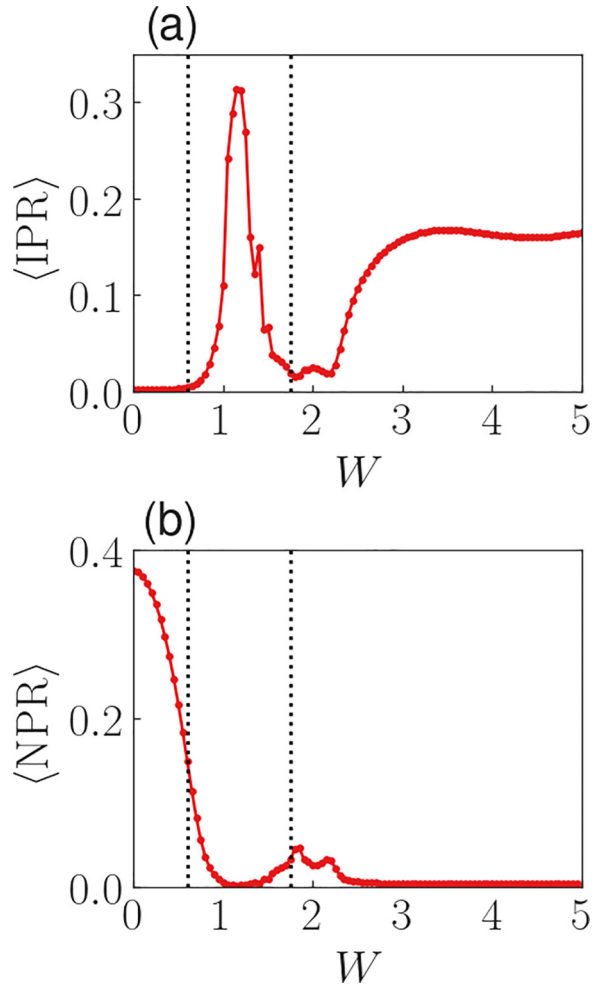

FIG. 8. Averages of Inverse Participation Ratio (IPR) and Normalized Participation Ratio (NPR), namely, (a) $\langle \text{IPR} \rangle$ and (b) $\langle \text{NPR} \rangle$ are plotted as a function of the disorder strength. Below $W = 0.6$, the midgap states are extended while being localized above that. However, around $W = 1.75$, both $\langle \text{IPR} \rangle$ and $\langle \text{NPR} \rangle$ exhibit finite nonzero values, indicating a possible multifractal state during phase transition. The two dotted lines demarcate the regime where the quadrupole moment is nontrivial.

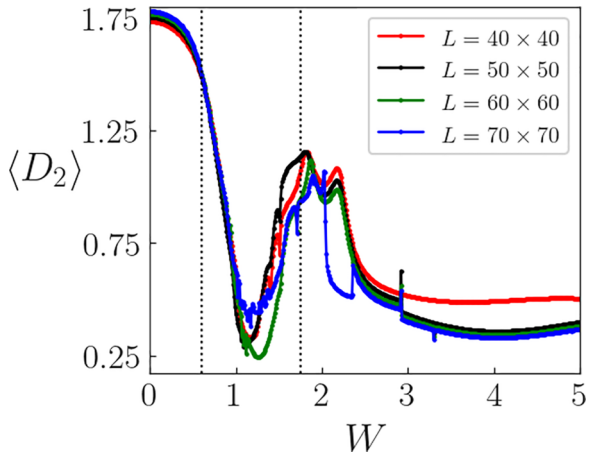

FIG. 9. The average fractal dimension $\langle D_2 \rangle$ exhibits a value close to $D = 2$, for $W < 0.6$, representing a trivial delocalized phase. In the topological regime, however, it approaches 0. During the phase transition (around $W = 1.75$), $\langle D_2 \rangle$ assumes a value between 0 and 2, thus providing concrete evidence of a multifractal phase. The calculations have been repeated for different system sizes to eliminate any possible finite-size effect, as shown in the figure.

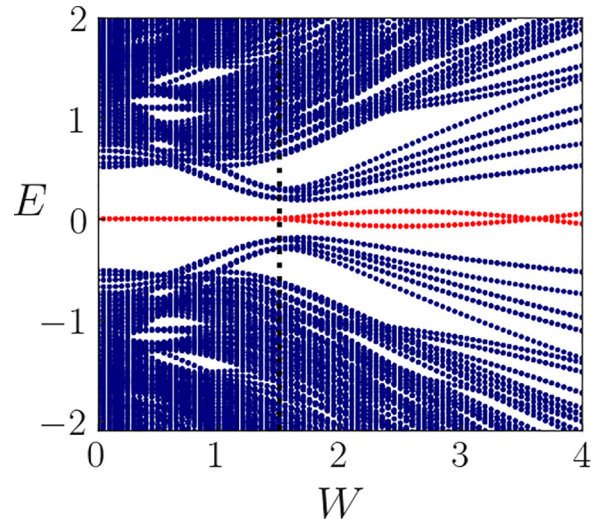

FIG. 10. The band structure of the Benalcazar-Bernevig-Hughes (BBH) model as a function of the disorder strength W for $\frac{\gamma}{\lambda} = 0.5$. It is observed that the in-gap states that are depicted in red remain confined at zero energy if $W \leqslant 1.5$.

Here, $L = L_x = L_y$ refers to the length of the system along the x or y direction. We again plot the average value of D_2 for the four midgap states as a function of the disorder strength in Fig. 9. Here, $\langle D_2 \rangle$ shows a value ∼2 and 0 for the regimes $W < 0.6$ and $W > 0.6$, respectively, which is consistent with the extended and localized nature of the mid-gap states. However, around $W = 1.75$, where the topological phase transition occurs, the value of $\langle D_2 \rangle$ lies distinctly between the two extremes, that is, $0 < D_2 < D$. Thus, it is evident that, close to the transition from a topological to a trivial phase, the zero-energy states acquire a fractal nature before getting completely localized again. The calculations have been repeated for various system sizes, and they provide robust evidence for the inferences made above.

B. Clean limit: Topological phase

1. Topological properties

We now focus on the effect of disorder on the topological properties of the BBH model, starting within a regime which is nontrivial in the clean limit. We fix the value of $\frac{\gamma}{\lambda}$ at 0.5, which originally corresponds to a quadrupolar TI [Fig. 2(a)]. The bulk band structure is similarly plotted as a function of the disorder strength W (Fig. 10). We observe that the in-gap states remain confined to zero energy until $W = 1.5$, beyond which they shift, indicating a possible destruction of the topological feature due to the imposed disorder. This is further confirmed by the quadrupole moment, which shows a transition to triviality at $W = 1.5$ (Fig. 11). Furthermore, the distribution of the excess charge at $W = 1.0$ shows charge accumulation of $\pm\frac{e}{2}$ at alternate corners like the previous case [Fig. 12(a)]. Beyond $W = 1.5$ [as shown in Fig. 12(b) for $W = 2.1$], there is negligible charge accumulation in the system, which is expected from a system with trivial quadrupole moment (Fig. 12). All the calculations have been done on a 40×40 square supercell.

2. Localization properties

To study the localization of the in-gap states, we again resort to a study of IPR and NPR as a function of W (Fig. 13). Interestingly, the system persists in a localized regime deep within the topological as well as the trivial phase. However, near the transition point, the states tend toward delocalization. This is exhibited by a sudden dip (spike) in the value of ⟨IPR⟩ (⟨NPR⟩) around the transition point at $W = 1.5$. Furthermore, finite and nonzero values of both ⟨IPR⟩ and ⟨NPR⟩ around the transition point indicate that the in-gap states might show possible multifractality. To confirm this, we resort to the evaluation of the fractal dimension D_2 [Eq. (9)]. We observe that D_2 exhibits a value ∼0.4, indicating a localized phase on both sides away from the transition point (Fig. 14). However,

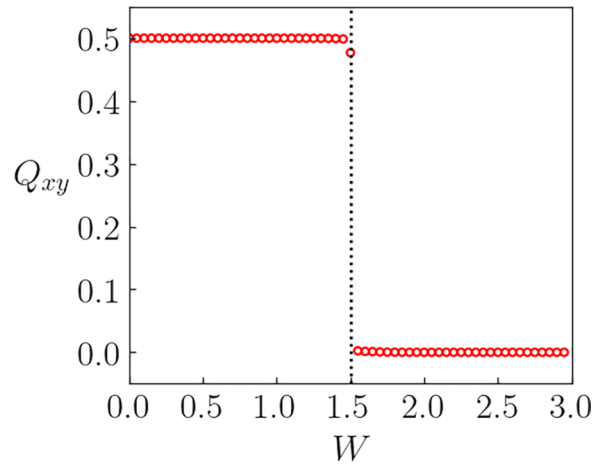

FIG. 11. The quadrupole moment Q_{xy} shows a behavior that accurately reciprocates the behavior of the band structure in Fig. 10. Here, Q_{xy} remains affixed at 0.5, indicating a topological phase, for the regime $W \leqslant 1.5$. Beyond this point, the system gets trivialized.

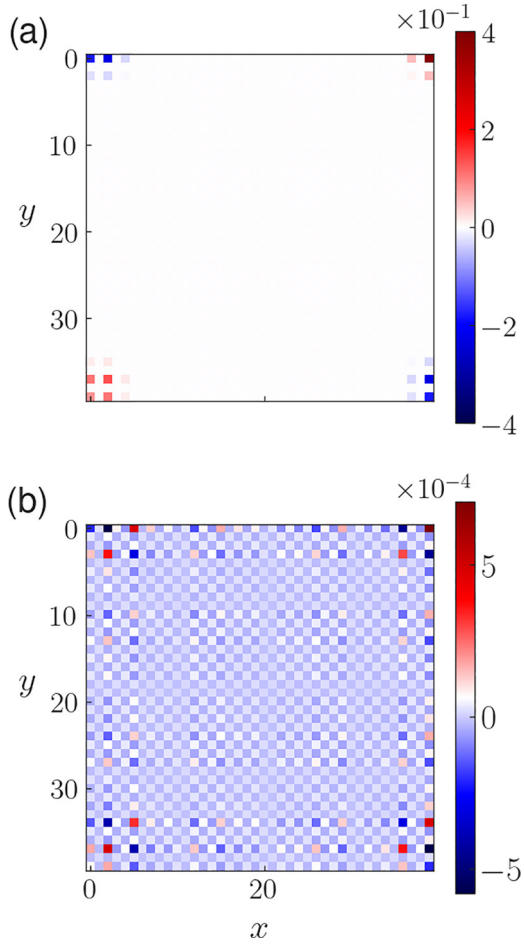

FIG. 12. The distribution of excess charge on a square supercell of size 40×40 for (a) $W = 1.0$ and (b) $W = 1.8$. Evidently, for $W \leqslant 1.5$, the system persists in the second-order quadrupolar phase.

around the transition point, $D_2 \in (0, 2)$; more specifically, $D_2 \sim 1.0$ near $W = 1.5$, thus indicating a multifractal phase.

IV. CONCLUSIONS

We observe a topological phase transition induced purely by QP disorder inculcated in the hopping amplitude of the BBH model. The quadrupole moment shows a restored topological phase as a function of the disorder strength in the regime where the clean system shows completely trivial behavior. The band structure of the BBH model under OBC also shows the emergence of zero-energy in-gap states in exact correspondence with the quadrupole moment, thus providing clear evidence of a second-order topological phase. Furthermore, the distribution of charge at the corners of the square supercell also shows a pattern that is suggestive of the bulk quadrupole topology. A localization study done on the midband states shows three different phases, namely, trivial delocalized, topological localized, and Anderson localized phases. The fractal dimension D_2 shows that, near the transition from the topological to the trivial localized phase, the system becomes multifractal, which

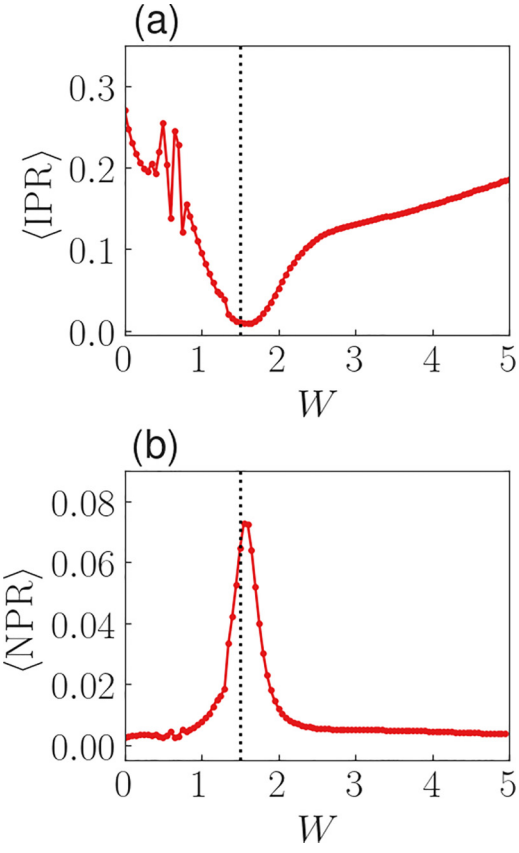

FIG. 13. The variation of (a) ⟨IPR⟩ and (b) ⟨NPR⟩ shows that the system is localized both in the topological ($W \leqslant 1.5$) and in the trivial ($W > 1.5$) phase. However, the dip(spike) in the value of ⟨IPR⟩ (⟨NPR⟩) around $W = 1.5$ hints at a topological phase transition.

is characterized by a value of D_2 between 0 and D. A similar phenomena occurs when we study the system as a function of disorder starting from a clean limit that is topological. Here, the disorder drives the in-gap states from being

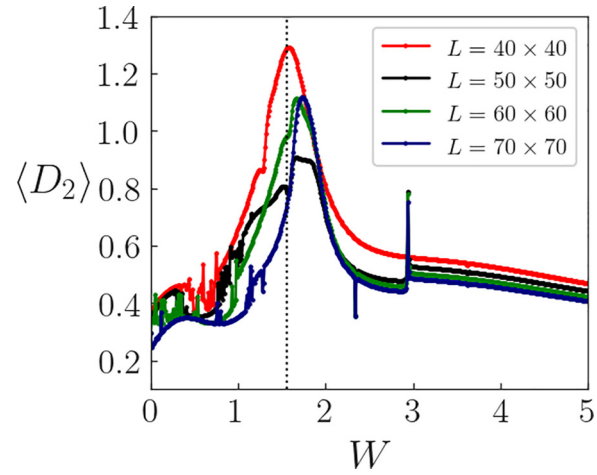

FIG. 14. The fractal dimension D_2 shows that the in-gap states exhibit a multifractal nature near the transition point $W = 1.5$ while being localized both in the trivial and the topological phases.

topologically localized to Anderson localized, corresponding to higher values of the disorder strength W. The point of transition is again host to a multifractal phase characterized by finite nonzero values of both ⟨IPR⟩ and ⟨NPR⟩. The fractal dimension D_2 provides further concrete evidence for this multifractality.

ACKNOWLEDGMENTS

One of the authors (S.L.) acknowledges the Ministry of Education (MOE), Government of India for providing financial support for her research work through the Prime Minister's Research Fellowship (PMRF) May 2022 scheme.

[1] M. Z. Hasan and C. L. Kane, Colloquium: Topological insulators, Rev. Mod. Phys. **82**, 3045 (2010).

[2] X.-L. Qi and S.-C. Zhang, Topological insulators and superconductors, Rev. Mod. Phys. **83**, 1057 (2011).

[3] M. Z. Hasan and J. E. Moore, Three-dimensional topological insulators, Annu. Rev. Condens. Matter Phys. **2**, 55 (2011).

[4] J. E. Moore, The birth of topological insulators, Nature (London) **464**, 194 (2010).

[5] B. A. Bernevig, T. L. Hughes, and S.-C. Zhang, Quantum spin Hall effect and topological phase transition in HgTe quantum wells, Science **314**, 1757 (2006).

[6] M. König, S. Wiedmann, C. Brune, A. Roth, H. Buhmann, L. W. Molenkamp, X.-L. Qi, and S.-C. Zhang, Quantum spin Hall insulator state in HgTe quantum wells, Science **318**, 766 (2007).

[7] K. Deng, G. Wan, P. Deng, K. Zhang, S. Ding, E. Wang, M. Yan, H. Huang, H. Zhang, Z. Xu *et al.*, Experimental observation of topological Fermi arcs in Type-II Weyl semimetal $MoTe_2$, Nat. Phys. **12**, 1105 (2016).

[8] A. A. Burkov and L. Balents, Weyl semimetal in a topological insulator multilayer, Phys. Rev. Lett. **107**, 127205 (2011).

[9] G. Xu, H. Weng, Z. Wang, X. Dai, and Z. Fang, Chern semimetal and the quantized anomalous Hall effect in $HgCr_2Se_4$, Phys. Rev. Lett. **107**, 186806 (2011).

[10] K. Zhang, M. Yan, H. Zhang, H. Huang, M. Arita, Z. Sun, W. Duan, Y. Wu, and S. Zhou, Experimental evidence for Type-II Dirac semimetal in $PtSe_2$, Phys. Rev. B **96**, 125102 (2017).

[11] N. Levy, T. Zhang, J. Ha, F. Sharifi, A. A. Talin, Y. Kuk, and J. A. Stroscio, Experimental evidence for *s*-wave pairing symmetry in superconducting $Cu_xBi_2Se_3$ single crystals using a scanning tunneling microscope, Phys. Rev. Lett. **110**, 117001 (2013).

[12] Y. Ando, K. Segawa, S. Sasaki, and M. Kriener, Experimental studies of the topological superconductor $Cu_xBi_2Se_3$, J. Phys.: Conf. Ser. **449**, 012033 (2013).

[13] T. H. Hsieh, H. Lin, J. Liu, W. Duan, A. Bansil, and L. Fu, Topological crystalline insulators in the SnTe material class, Nat. Commun. **3**, 982 (2012).

[14] Y. Tanaka, Z. Ren, T. Sato, K. Nakayama, S. Souma, T. Takahashi, K. Segawa, and Y. Ando, Experimental realization of a topological crystalline insulator in SnTe, Nat. Phys. **8**, 800 (2012).

[15] F. Schindler, A. M. Cook, M. G. Vergniory, Z. Wang, S. S. P. Parkin, B. A. Bernevig, and T. Neupert, Higher-order topological insulators, Sci. Adv. **4**, eaat0346 (2018).

[16] E. Khalaf, Higher-order topological insulators and superconductors protected by inversion symmetry, Phys. Rev. B **97**, 205136 (2018).

[17] A. Matsugatani and H. Watanabe, Connecting higher-order topological insulators to lower-dimensional topological insulators, Phys. Rev. B **98**, 205129 (2018).

[18] S. Franca, J. van den Brink, and I. C. Fulga, An anomalous higher-order topological insulator, Phys. Rev. B **98**, 201114(R) (2018).

[19] S. Manna, S. Nandy, and B. Roy, Higher-order topological phases on fractal lattices, Phys. Rev. B **105**, L201301 (2022).

[20] S. Traverso, M. Sassetti, and N. T. Ziani, Role of the edges in a quasicrystalline Haldane model, Phys. Rev. B **106**, 125428 (2022).

[21] F. Schindler, Z. Wang, M. G. Vergniory, A. M. Cook, A. Murani, S. Sengupta, A. Yu. Kasumov, R. Deblock, S. Jeon *et al.*, Higher-order topology in bismuth, Nat. Phys. **14**, 918 (2018).

[22] R. Noguchi, M. Kobayashi, Z. Jiang, K. Kuroda, T. Takahashi, Z. Xu, D. Lee, M. Hirayama, M. Ochi, T. Shirasawa *et al.*, Evidence for a higher-order topological insulator in a three-dimensional material built from van der Waals stacking of bismuth-halide chains, Nat. Mater. **20**, 473 (2021).

[23] W. A. Benalcazar, B. A. Bernevig, and T. L. Hughes, Electric multipole moments, topological multipole moment pumping, and chiral hinge states in crystalline insulators, Phys. Rev. B **96**, 245115 (2017).

[24] W. A. Benalcazar, B. A. Bernevig, and T. L. Hughes, Quantized electric multipole insulators, Science **357**, 61 (2017).

[25] C.-A. Li and S.-S. Wu, Topological states in generalized electric quadrupole insulators, Phys. Rev. B **101**, 195309 (2020).

[26] Y.-B. Yang, K. Li, L.-M. Duan, and Y. Xu, Type-II quadrupole topological insulators, Phys. Rev. Res. **2**, 033029 (2020).

[27] The classical relation refers to

$$p_x^{\text{edge}\pm y} = p_y^{\text{edge}\pm x} = q^{\text{corner}\pm x,\pm y} = |Q_{xy}|.$$

Here, $p^{\alpha}_{x(y)}$ refers to the $x(y)$ component of polarization at the boundary of the supercell with normal vector pointing along the direction α. Also, q and Q refer to the charge accumulation at the corners (again specified by the coordinates mentioned in the superscript) and the bulk quadrupole moment, respectively. For more details, please see Ref. [23].

[28] Y.-L. Tao, J.-H. Wang, and Y. Xu, Quadrupole insulator without corner states in the energy spectrum, arXiv:2307.00486.

[29] H. Hu, B. Huang, E. Zhao, and W. V. Liu, Dynamical singularities of Floquet higher-order topological insulators, Phys. Rev. Lett. **124**, 057001 (2020).

[30] T. Nag, V. Juričić, and B. Roy, Out of equilibrium higher-order topological insulator: Floquet engineering and quench dynamics, Phys. Rev. Res. **1**, 032045(R) (2019).

[31] Y. Tian, Z. Tan, W. Zhang, X. Han, and C. Cho, Analogous quadrupole topology induced by non-hermiticity, Phys. Rev. B **107**, 094107 (2023).

[32] C.-A. Li, B. Fu, Z.-A. Hu, J. Li, and S.-Q. Shen, Topological phase transitions in disordered electric quadrupole insulators, Phys. Rev. Lett. **125**, 166801 (2020).

[33] Y.-B. Yang, K. Li, L.-M. Duan, and Y. Xu, Higher-order topological Anderson insulators, Phys. Rev. B **103**, 085408 (2021).

[34] Y.-B. Yang, J.-H. Wang, K. Li, and Y. Xu, Higher-order topological phases in crystalline and non-crystalline systems: A review, J. Phys.: Condens. Matter **36**, 283002 (2024).

[35] A. Štrkalj, E. V. H. Doggen, and C. Castelnovo, Coexistence of localization and transport in many-body two-dimensional Aubry-André models, Phys. Rev. B **106**, 184209 (2022).

[36] A. Szabó and U. Schneider, Mixed spectra and partially extended states in a two-dimensional quasiperiodic model, Phys. Rev. B **101**, 014205 (2020).

[37] N. Mott, The mobility edge since 1967, J. Phys. C **20**, 3075 (1987).

[38] G. A. Domínguez-Castro and R. Paredes, The Aubry-André model as a hobbyhorse for understanding the localization phenomenon, Eur. J. Phys. **40**, 045403 (2019).

[39] J. Biddle, B. Wang, D. J. Priour, Jr., and S. Das Sarma, Localization in one-dimensional incommensurate lattices beyond the Aubry-André model, Phys. Rev. A **80**, 021603 (2009).

[40] Q.-B. Zeng, Y.-B. Yang, and Y. Xu, Higher-order topological insulators and semimetals in generalized Aubry-André-Harper models, Phys. Rev. B **101**, 241104(R) (2020).

[41] B. Kang, K. Shiozaki, and G. Y. Cho, Many-body order parameters for multipoles in solids, Phys. Rev. B **100**, 245134 (2019).

[42] F. Evers and A. D. Mirlin, Fluctuations of the inverse participation ratio at the Anderson transition, Phys. Rev. Lett. **84**, 3690 (2000).

[43] S. Roy, S. N. Nabi, and S. Basu, Critical and topological phases of dimerized Kitaev chain in presence of quasiperiodic potential, Phys. Rev. B **107**, 014202 (2023).

[44] X. Li and S. Das Sarma, Mobility edge and intermediate phase in one-dimensional incommensurate lattice potentials, Phys. Rev. B **101**, 064203 (2020).